PIC Simulation of High Specific Impulse Hall Effect Thruster*†

Vincent Blateau, Manuel Martinez-Sanchez, Oleg Batishchev and James Szabo
Massachusetts Institute of Technology
77 Massachusetts Avenue
Cambridge, MA 02139
617-253-7485
blateau@mit.edu

IEPC-01-037

A previously developed computational method, which treats all particles in the plasma kinetically, is applied for a study of the effects of increasing the voltage beyond the well-established range around 300V (for Xenon). Although some additional code development is still necessary to improve absolute accuracy, several important trends and effects are identified through these calculations. If the magnetic field is kept constant, the overall anode efficiency is found to increase at first, peak at about 600V, then decrease at higher voltages. On the other hand, if B is optimized at each voltage, the efficiency increases continuously with V. The detailed physics behind this behavior are identified. The second-ion fraction (Xe^{++}/Xe^{+}) increases rapidly at first, but nearly saturates with further voltage increases. The electron temperature approaches proportionality with voltage, since metallic walls (TAL style) were assumed, and secondary electron emission was ignored.

1. Introduction

There is increased interest [1] in extending the range of mission applicability of Hall thrusters through increases in their operating specific impulses, and, if possible, of their efficiency. The experimental evidence which is beginning to appear about higher voltage operation [2,3,4,5,6] confirms that simply raising voltage at constant flow rate (with a re-optimization of magnetic field depending on voltage) does indeed lead to higher thrust, and higher efficiency as well. Since this is obtained with thrusters, which were originally designed for V~300 Volts, the results are encouraging, but difficulties are expected on at least two accounts: overheating and life reduction. Some innovative designs have been suggested for high-voltage application, such as two-stage thrusters [7,8,9], and one can generally expect that even the conventional designs, will have to be re-optimized in their dimensions and proportions for this purpose. This task will require a concerted experimental and theoretical effort to extend our understanding of the basic thruster physics so as to cover the higher-energy regime. We, with NASA-Glenn support, have recently initiated at MIT and BUSEK a research program in this direction. This paper reports some of the initial computational results of this program.

The method used is a full Particle-in-Cell code developed by J. Szabo at MIT and reported previously [10,11,12]. The method and the thruster configuration used are summarized in Section 2.

Section 3 presents a summary of the aggregate results and their trends, plus a comparison of the 2-D distributions (plasma density, temperature, ionization, etc) at two different voltages.

Section 4 contains more detailed analyses and discussions of some of the salient trends found. Sec. 4.1 illustrates changes vs. mass flow rate at fixed voltage. Section 4.2 (and Appendix A) breaks the efficiency down to its various components, and discusses their individual trends vs. voltage.

We conclude in Sec. 5 with a summary of main results and some recommendations for further research.

* Presented as Paper IEPC-01-037 at the 27th International Electric Propulsion Conference, Pasadena, CA, 15-19 October, 2001.

2. Method and Configuration

2.1 Code used

General characteristics

The code used was developed by James Szabo at MIT for his PhD degree [11]. It is a full particle-in-cell (PIC) code with two dimensions in space, three dimensions in velocity. It includes single and double ions along with neutral excitation. A few tricks are used to speed up the computation:

- An artificial permittivity $\varepsilon' = \gamma^2 \varepsilon_0$ is used to decrease both the Debye length and plasma time by a factor γ. Because of this, the quasi-neutrality is not strictly maintained, especially in the acceleration region.
- An artificial mass ratio $\frac{M'}{M} = f < 1$ increases the neutral and ion speed by a factor $\sqrt{1/f}$. This artificial ratio speeds up the convergence of the code, governed by heavy particles. Cross-sections are also increased by this factor, to correct the various rates and compensate for the higher neutral velocity.
- Computation particles have an average size of ~10^6 particles, and neutral particles have a relative weight of 50 compared to other particles.

Particle injection and boundary conditions

Neutrals are injected at the anode with a half-maxwellian distribution of temperature .1eV; electrons coming from the cathode (outside the simulation region) are injected at the right hand side at a rate to maintain local quasi-neutrality. They have a velocity set by the potential at the point they are created and the cathode temperature [11, section 3.20.3].

At the centerline, particles are specularly reflected. At the metallic walls (including the anode) however, electrons are deleted, ions lose their charge(s). They are re-emitted as neutrals in a random direction with half their initial kinetic energy. Neutrals hitting the wall are re-emitted at the wall temperature (700K for the metallic wall, .1eV for the anode) with a half-maxwellian distribution.

The charge balance at the floating metallic wall determines the wall potential, using a capacitance $C = 10^{-10} F$. Other boundaries for the Poisson solver are symmetry at the centerline, anode potential at the anode, zero longitudinal E-field at the vertical right hand side. The potential at the upper right hand side is calculated using a sheath model between the wall (at the wall potential), and the right hand side corner (at the cathode potential).

Particle motion and collisions

Particles are moved forward by a leapfrog algorithm; neutrals are moved every 10 ion and electron time steps only.

Collisions modeled include electron-neutral elastic scattering, neutral excitation (one lumped level only), neutral single and double ionization; single ion additional ionization, electron-electron and electron-ion Coulomb collisions (Fokker-Planck algorithm), ion-neutral charge exchange and elastic scattering. Cross-section values can be found in [12] and [11]. Bulk recombination is not considered.

2.2 Thruster modeled

The thruster modeled is the 50-Watt mini-TAL thruster, built at MIT by Khayms, except that the anode is as modified by Szabo [11] to reduce magnetic line interception. The design mass flow rate and voltage are .13 mg/s and 300V.

The artificial parameters used are $f = 1/2{,}500$ and γ=10. The 87*49 grid (Fig. 1) resolves the modified Debye length $d = \gamma\sqrt{\frac{\varepsilon_0 k T_e}{e^2 n_e}}$; the time step used is smaller than the modified plasma time: the new limit is the electron gyro motion frequency

$$\omega_{Larmor} = \frac{eB}{m_e} > \frac{1}{\gamma}\sqrt{\frac{e^2 n_e}{m_e \varepsilon_0}} = \omega_p .$$

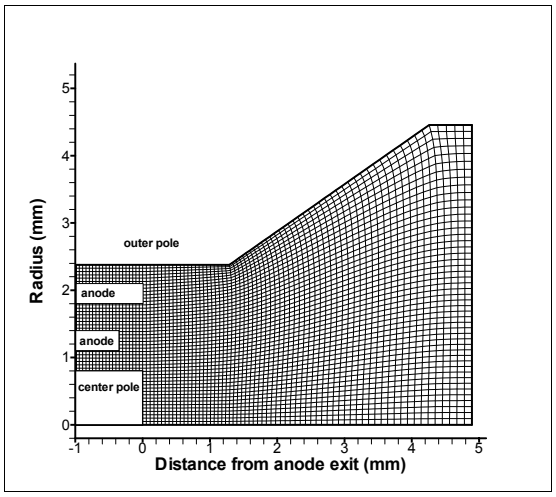

Figure 1 - Computational grid

A full case takes about 80,000 iterations to converge, the convergence criteria being the total neutral mass in the simulation. However, for cases close to each other, we used converged solutions re-ran with modified parameters. This enables us to achieve convergence in 20,000 iterations only (about 12 hours of CPU time on a Pentium IV 1.5GHz PC).

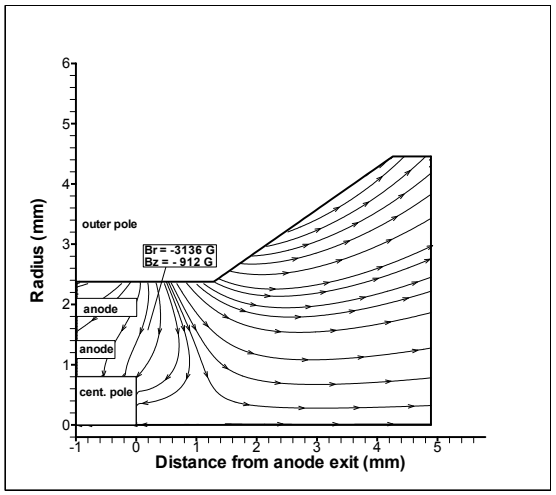

Figure 2 - Nominal magnetic field lines

In this paper, different voltages have been tested: 300, 600, 900 and 1200 Volts, for a mass flow rate of 0.1mg/s. For each voltage, the optimal relative B-field, relative to the nominal design B-field (Fig. 2) has been found. One case at another mass flow: 600V, 0.167 mg/s, nominal B-field, has been run. The results are presented in Table 2.

3. Performance results

3.1 Global performance parameters

The main parameters characterizing the thruster's operation at a variety of conditions are collected together in Table 2. Except for one case at V= 600 V, the rest are all at the normal flow rate $m = 0.1mg/s$. At each voltage the magnetic field was optimized (coarsely) with respect to overall efficiency; for 600V, the nominal B field was found to be approximately optimal. The results of [6] suggest that B_{opt} scales as $V^{1/2}$ for SPT-type thrusters, and there is some theoretical justification for this scaling, in that this would preserve the Larmor radius of electrons with speeds proportional to $V^{1/2}$. Our results (Fig. 3) seem to depart from this law towards B ~ V, which is the behavior found theoretically in [13] to describe the upper limit of the existence domain for steady flow solutions in a TAL-type of thruster (no strong wall losses).

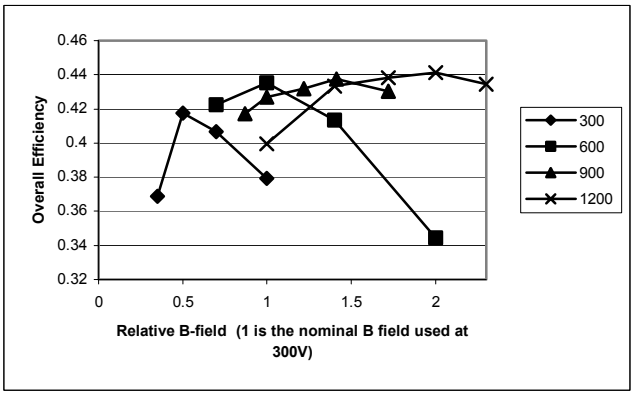

Figure 3 – Efficiency at different B-fields for different voltages

Table 2 indicates that the various computed currents stay fairly constant as V is varied, except for some noticeable increase in the anode (or cathode) current between 300V and 600V.

Table 1. Computed contributions of double ions to mass flow, beam current and thrust (for 0.1 mg/s).

V (Volts)	300	600	900	1200
m^{++}/m	0.088	0.123	0.145	0.168
I_b^{++}/I_b	0.202	0.247	0.271	0.303
F^{++}/F	0.149	0.178	0.196	0.218

The (constant) mass flow is broken down in Table 2 into its constituents as they leave the engine: simple

ions, double ions and neutrals. The most interesting part of these results is the double ion fraction. This is extracted into Table 1, together with the results for thrust contributed by the various species.

More will be said about these results in Sec. 4, but it is worth pointing out at this time that the various double ion contributions increase strongly with voltage only at the low end of the range, and tend to saturate to nearly constant values at the higher voltages.

The thrust and specific impulse increase roughly as $V^{1/2}$, as expected. The mean electron temperature ($<T_e>$, in eV) is shown in the next line of Table 2, and also in Fig. 4. The variation with voltage approaches proportionality at high V, but is slower than that initially. This may imply reductions of beam divergence between V=300V and, say, 600V, because the radial ion thermal speed will increase less rapidly than their axial speed, but our computation cannot accurately extend out to the plume to verify this.

The potential of the outer channel wall is computed assuming the wall is metallic and electrically floating. Table 2 shows that this wall remains very close to cathode potential throughout. This is in accordance with TAL experimental evidence and is probably due to the fact that some magnetic lines from the cathode region intercept that wall (Fig. 2).

The particle number densities at a selected point are also indicated in Table 2. There is some randomness in these "typical" results, due to motion of the ionization region with respect to the chosen point, but we can observe a general trend for ion densities to decrease with voltage, presumably as a consequence of their higher speeds (and despite somewhat increased ionization fractions). The neutral density falls faster, since both effects add together for them. A similar message is conveyed by the total mass of neutrals and ions in the simulation, also reported in the table.

The last section of Table 2 concerns the various pieces that go into the calculation of overall efficiency, defined as $\eta = T^2/(2mI_aV)$. We will here only comment on the overall efficiency itself (last line in Table 2), and leave a more detailed discussion for Sec. 4. If we compare the cases run at "nominal B field" (Fig. 5), we can see a clear optimum at V=600V ($\eta \cong$ 0.419), with a rapid rise from 300 to 600V and a slower decrease beyond 600V. The comparison at near-optimum B field (Fig. 6) still shows a monotonic increase of efficiency with voltage, although with a noticeable wakening of the trend between 600 and 900V. This is similar to the experimental data of [3]. In [4] (single stage case), there is actually a small decreases in efficiency in the intermediate range, followed by increases at higher voltages. [5] and [6] show distinct optima near 600V.

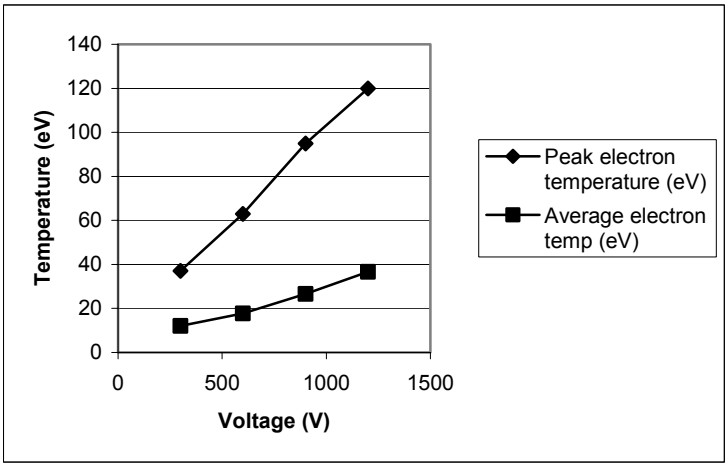

Figure 4 - Peak and average electron temperature for different voltages, at optimum B-fields

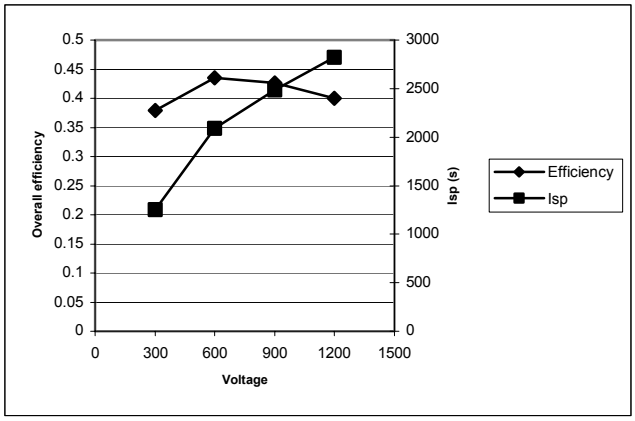

Figure 5 – Efficiency and Specific Impulse versus Voltage at constant B-field

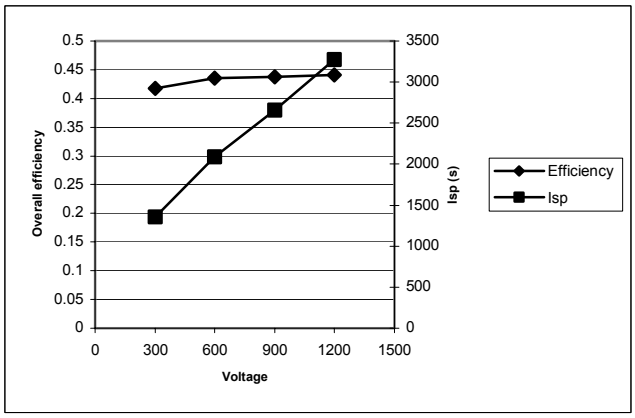

Figure 6 - Efficiency and Specific Impulse versus Voltage at optimum B-field

3.2 Spatial Distributions at two Voltages

For the voltages of 300V and 600V, at nominal Bfield, Figs. 7 through 13 summarize the (time-averaged) results for the main plasma quantities of interest.

Figs. 7a and 7b refer to electron temperature (ignoring the differences between $T_\perp$ and $T_\parallel$ which were reported in [10]–[12]). At 300 V, T_e is about 4eV near the cathode and inside the anode channel, and reaches about 40eV in the region of the anode opening. A secondary maximum of T_e can be seen along the thruster axis, where an intensely luminous "spike" is normally observed. For 600V (Fig. 7b) the peak temperatures reach 60eV.

The potential maps (Figs. 8a, 8b) are fairly similar in shape in both cases. The high field, or acceleration region, extends only about the width of the anode downstream, and fairly low potentials are seen beyond this point. However, the spike region, near the axis, also shows increased potentials, in both cases to about 40eV.

The electron densities are mapped in Figs. 6a and 6b. The most interesting observation is that the highest density is actually in the spike region, where it reaches about 8×10^{19} m^{-3}. This accounts for the strong luminosity of this region, which, however, is small in volume, as it lies so close to the axis. Its origin is mainly kinematical, a result of the crossing of many ion trajectories from all around the anode annulus. The principal plasma region is a ring in front of the anode, where n_e peaks at about 1.6×10^{19} m^{-3} for 300V, and about 1.3×10^{19} m^{-3} for 600V.

Figures 10-12 detail the various ionization processes. In Fig. 10, the first ion production is seen to peak in the main plasma ring near the anode, where both n_e and n_n as well as T_e are high. The peak value is lower at 600V than at 300V, reflecting the lower n_e and n_n principally. Fig. 11 shows production of double ions from neutrals following $n + e \rightarrow i^{++} + 3e$. This process occurs fairly much concurrent with single-ion formation, since the same ingredients feed into both. Once again, the maximum rate is lower at the higher voltage.

By contrast, Fig. 12 shows that those double ions, which originate from single ions by $i^{+} + e \rightarrow i^{++} + 2e$ do so predominantly in the spike region. This is because of the very high first ion density in this region, while neutrals, absent there, are not involved. Altogether, both double ion production channels contribute about equally to the total, but their very different geometrical distribution has interesting and strong consequences, to be expanded upon in Sec. 4. We only advance here the observation that double ions from the second channel (Fig. 12) are created at very low potentials, and contribute little to thrust.

Finally, Fig. 13 details the rate for the one lumped neutral excited level population rate. It is assumed in the code that the corresponding excitation energy is fully lost by prompt radiative decay. As expected, this process is fairly similar in distribution to ionization, and, once again, it is seen to decrease in intensity as voltage increases.

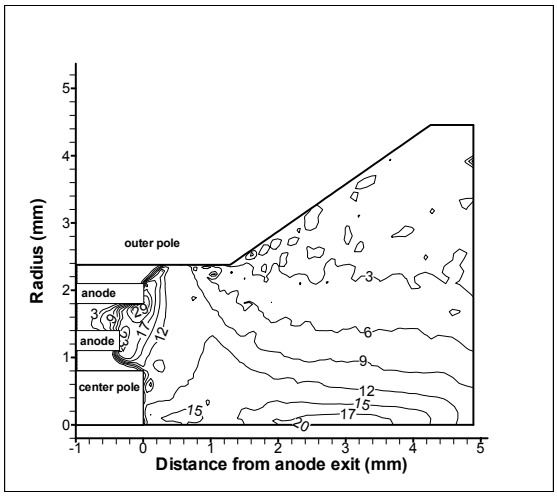

Figure 7a - Electron temperature in eV, voltage 300V

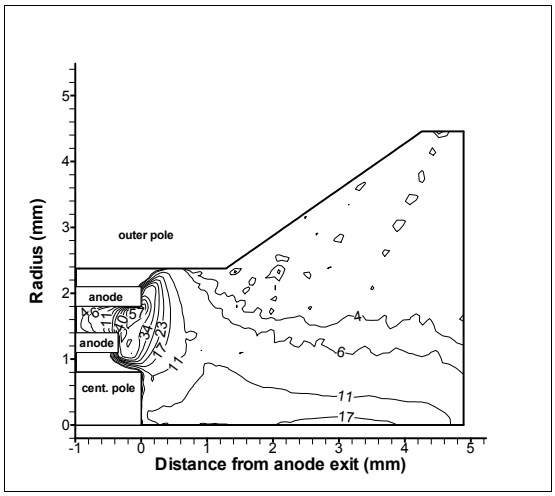

Figure 7b - Electron temperature in eV, voltage 600V

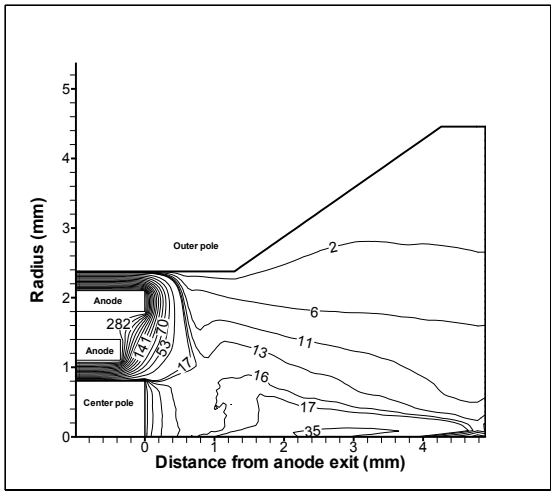

Figure 8a - Potential in V, voltage 300V

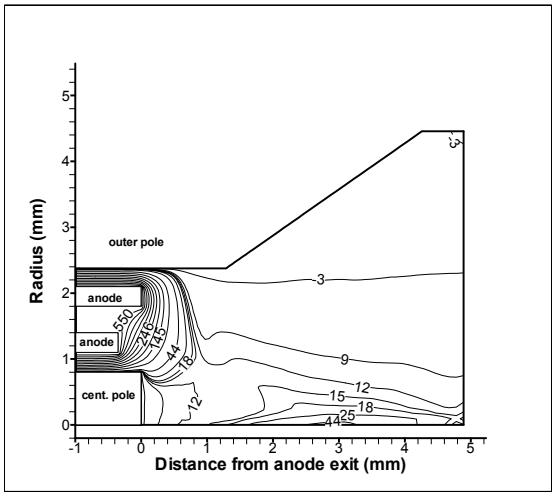

Figure 8b - Potential in V, voltage 600V

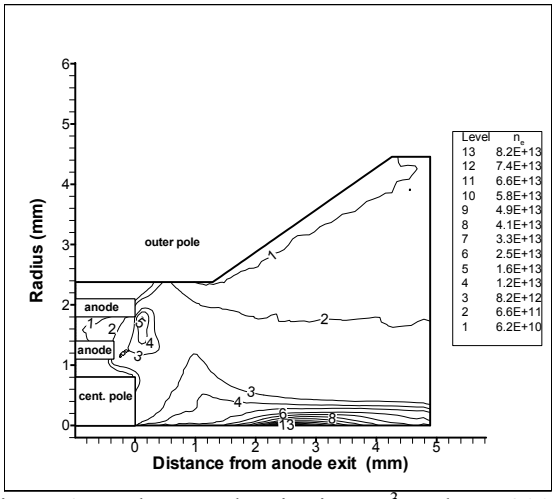

Figure 9a - Electron density in cm^{-3}, voltage 300V

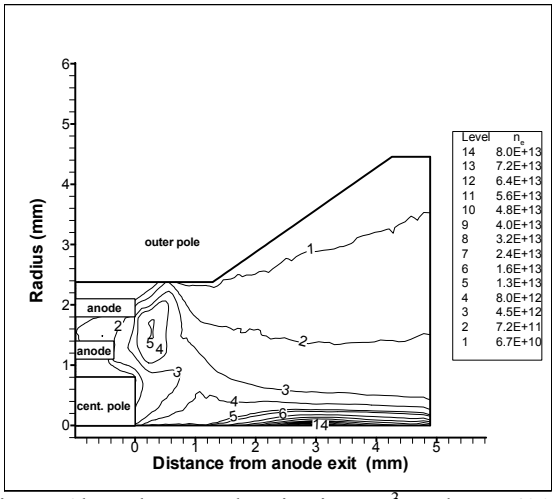

Figure 9b - Electron density in cm^{-3}, voltage 600V

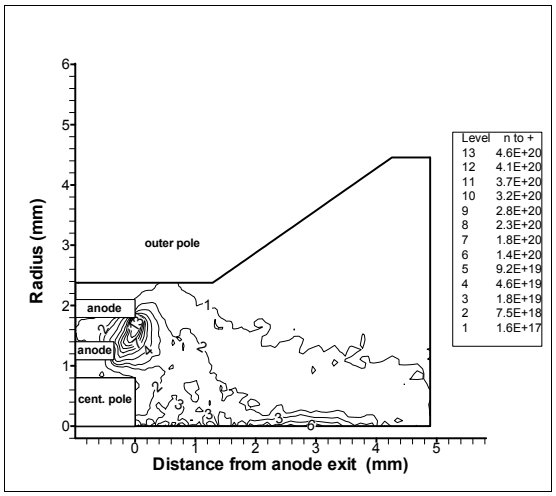

Figure 10a - Single ion creation from neutrals per unit volume in $cm^{-3}s^{-1}$, voltage 300V

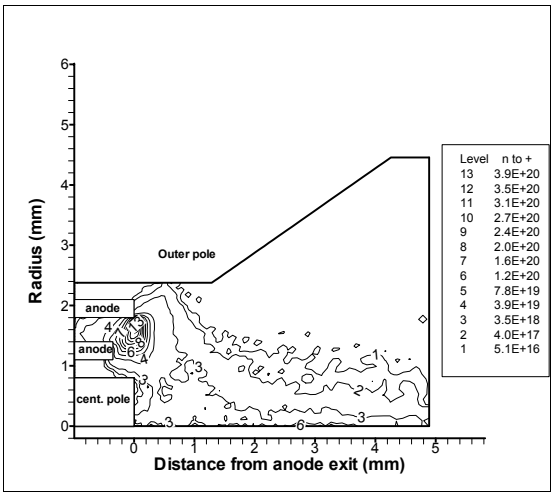

Figure 10b - Single ion creation from neutrals per unit volume in $cm^{-3}s^{-1}$, voltage 600V

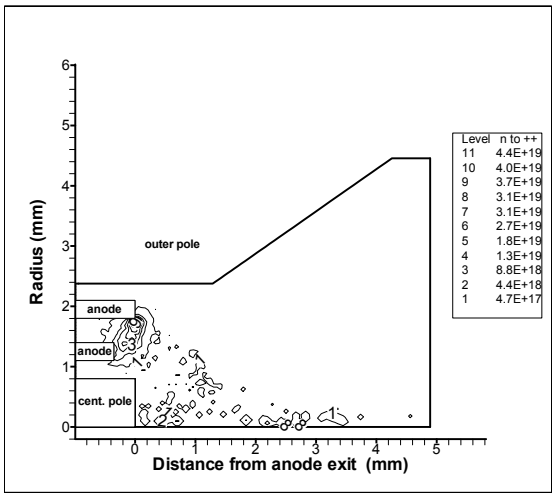

Figure 11a - Double ion creation from neutrals per unit volume in $cm^{-3}s^{-1}$, voltage 300V

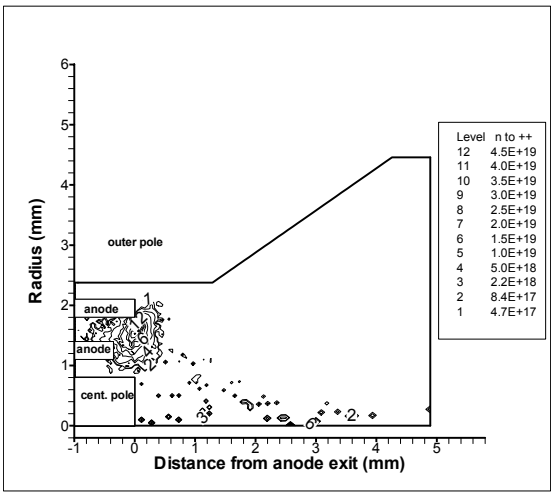

Figure 11b - Double ion creation from neutrals per unit volume in $cm^{-3}s^{-1}$, voltage 600V

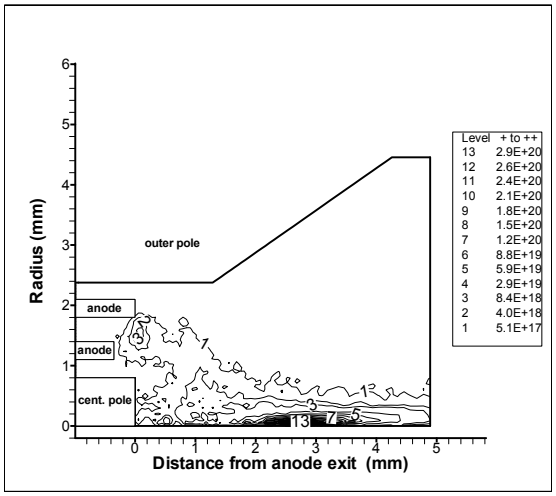

Figure 12a - Double ion creation from single ion per unit volume in $cm^{-3}s^{-1}$, voltage 300V

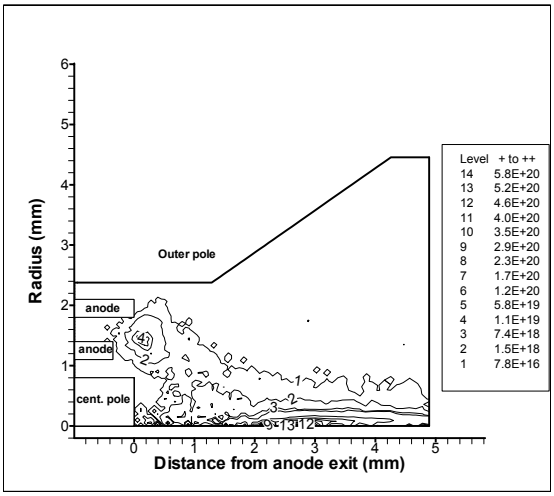

Figure 12b - Double ion creation from single ions per unit volume in $cm^{-3}s^{-1}$, voltage 600V

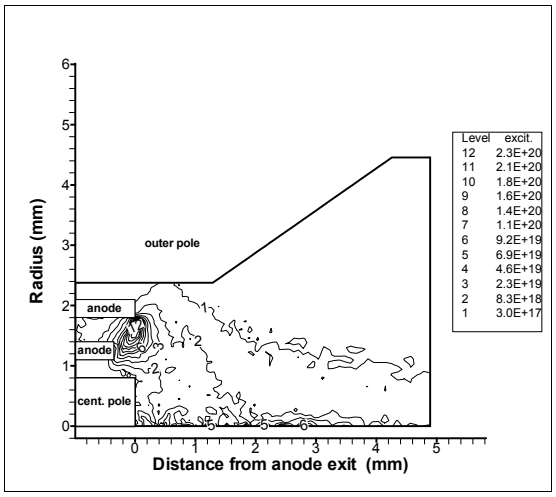

Figure 13a - Neutral excitation per unit volume in $cm^{-3}s^{-1}$, voltage 300V

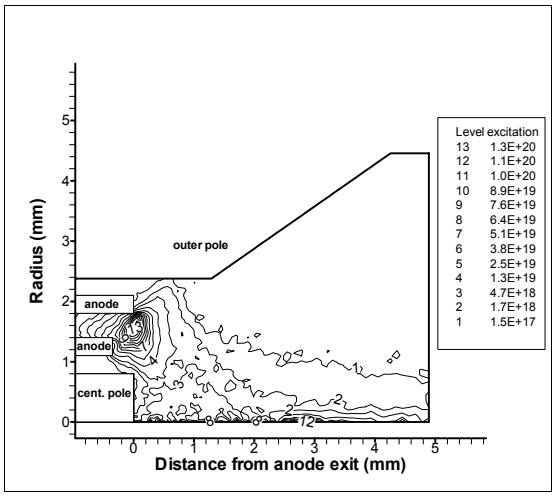

Figure 13b - Neutral excitation per unit volume in $cm^{-3}s^{-1}$, voltage 600V

4. Trends

4.1 Effects of mass flow changes

Table 2 contains two cases for V=600V, $B=B_{NOMINAL}$, one of which has $m = 0.1052 mg/s$ (nominally 0.1 mg/s), while the other has $m = 0.1875$ mg/s (nominally 0.167 mg/s). Because of the increased collisionality, one might expect the case with higher flow to show lower electron temperature and perhaps also lower double-ion fractions. Examination of the results in Table 1 shows in fact the opposite trends. This can be explained as follows: since n_e increases with m, the mean free path of a given neutral between ionizing collisions decreases, and neutrals are more likely to be ionized. This is borne out in the result by the larger ratio of total mass of ions to total mass of neutrals for the higher m, as well as by the densities at the central point. This then means that a given electron will collide with fewer neutrals, and will experience lower ionization and excitation energy losses. Since the energy source (the potential difference) has not changed, a higher electron temperature will result.

Regarding double ions, the ratio of their production rate to that of first ions is

$$\frac{n^{++}}{n^{+}} = \frac{k_{02}(T_e) n_n n_e + k_{12}(T_e) n^{+} n_e}{k_{01}(T_e) n_n n_e} = \frac{k_{02}(T_e)}{k_{01}(T_e)} + \frac{k_{12}(T_e)}{k_{01}(T_e)} \frac{n^{+}}{n_n} \qquad (1)$$

The small change in T_e is not a strong effect, since most electrons are well above threshold for these transitions at the prevalent high temperatures. The factor $\frac{n^{+}}{n_e}$ in the second term indicates therefore that there will be proportionally more double ions produced from first ions when m increases. Since the other production channel (from neutrals) will change little, we can expect an increased double ion fraction at higher flow, as indeed the table shows: 12.4% double ion mass flow fraction at 0.1 mg/s, vs. 18.1% at 0.167 mg/s. The other conclusion from Eq. (1) is that, because the double ions formed from first ions are mainly produced in the low-potential spike region, the mean velocity of double ions will be reduced as m increases. This is confirmed by the $\beta^{++} = \langle v_z{}^{++} \rangle / \langle v_z{}^{+} \rangle$ factors also listed in Table 2: 1.32 for the low-flow case, vs. 1.22 for the higher flow case (recall that β^{++} would be $\sqrt{2} = 1.414$ if double ions were created in the same region as single ions).

Finally, in terms of performance, there is a significant increase in specific impulse (Isp) and a small increase in efficiency at the higher flow rate. The higher Isp results from the higher proportion of the flow, which is in the form of ions, and especially of double ions. The higher efficiency is driven by the larger value of $\eta_e = I_b / I_a$, which in turn appears to result from the fact that many of the secondary electrons produced in the low-potential region by the process

$i^+ + e \rightarrow i^{++} + 2e$ actually pass downstream into the beam instead of back-streaming to the anode.

4.2 Analysis of Efficiency Changes vs Voltage

The introduction of second ionization in the simulation necessitates some redefinition of the familiar fractional efficiencies used for Hall thrusters. This is summarized in our Appendix A. In short, the overall (anode) efficiency is the product of four factors; (a) the "Dispersion Efficiency", which penalizes non-axial first ion discharge, (b) the "Acceleration Efficiency", which represents the ratio of the mean potential at which first ions appear to the applied voltage, (c) the "Electrical Efficiency", or ratio of beam to anode or cathode current, and (d) the "Effective Utilization Efficiency", which in the absence of double ions would reduce to the fraction of mass flowing out as ions; the double ions introduce a correction factor for this, which depends on the ratio of mean velocity of double ions to that of the single ions.

Upon examination of the relevant part of Table 2 (the last block of rows), the first striking piece of information is the value of the Electrical Efficiency, which remains in the neighborhood of unity, even higher in some cases. This means that the beam current is comparable to or larger than the anode current, which is not a familiar situation (values of 0.6-0.7 are common for this ratio). The implication is that a good number of secondary electrons from ionization events manage to leave with the ions and help neutralize the beam, without having to back-stream to the anode and be re-injected as cathode current. We have verified that this is indeed what the computation shows, and the inference is that this effect is due to the high rate of second ion creation from first ions in the spike region (Figs. 12), at potentials below about 30 Volt (Figs.8). Whether this is peculiar to this thruster's geometry (small ratio of inner to outer annulus ratio, which would tend to enhance the spike effect) needs to be resolved in future. Aside from the unexpected magnitude of this ratio, its trends are intelligible. For instance, if B is kept constant, the beam/anode current ratio decreases as voltage is raised. This indicates that electron back-streaming is being facilitated by the higher anode potentials. On the other hand, if we compare the B-field optimized cases, the ratio remains about constant, as the additional impedance keeps back-streaming in check.

Regarding the utilization efficiency (either for single ions or the corrected "effective" value), we can see in Table 2 that, both at constant B and for the B-optimized cases, the trend is to rise fairly rapidly between 300 and 600V, then to saturate at nearly constant values. This may be related to the increase of the electron temperature with voltage, which makes a strong impact on ionization at the lower end of the voltage range. At low T_e, a temperature increase moves more ions into the high cross-section range; at the higher temperatures, most electrons are beyond the ionization threshold, and are in fact moving into the decreasing part of the cross-section curve. For related reasons, we have noticed that the excitation/radiation losses become a smaller fraction of the total electron energy balance at higher voltages.

As noted, total (single+double) ion utilization efficiency rises steadily from under 80% to more than 90% as applied voltage is increased from 300V to 1.2kV. The average degree of gas ionization remains at about 4%, with a slight tendency to decrease. This indicates that the ion velocity is increasing faster than the neutral velocity, and so we can conclude that charge-exchange is not an important factor overall.

Interestingly enough, the degree of xenon ionization at the chosen fixed point in the anode layer changes drastically from ~7% to ~55% as the anode potential rises, while plasma and gas densities drop by factors 2 and 20, respectively. This shows that the ionization front is penetrating closer to the anode as the voltage increases, so the test point is in the highly ionized region at high voltages.

In connection with this, we can examine the behavior of the Acceleration Efficiency. At constant B-field, and at least above 600V, this quantity decreases with voltage, probably because ionization begins whenever electrons have gathered enough energy, and this happens at a lower fraction of the total potential when this potential is high. In contrast, for the B-optimized cases the acceleration efficiency increases in the same voltage range; this appears to be consistent with our earlier observation that the ionization layer is moving closer to the anode, and hence to the anode potential, in those cases.

Because ion utilization efficiency stays high, the plasma production rate (if neutral wall recycling is low) has to be about the same:

$$\int N \frac{\int \sigma_I f_e \mathrm{dv}}{\int f_e \mathrm{dv}} \sqrt{T_e} n_e \mathrm{dr} \approx const. \qquad (2)$$

From Fig. 4 one can see that the electron temperature, T_e, goes up by a factor of 3. As i) the electron temperature is always above ionization potential (~12eV), ii) the electron impact ionization cross-section saturates and even goes back at higher energies (see relevant data in [12]), and iii) PIC simulations [10,11] show that the electron distribution function (EDF) is close to Maxwellian, we may assume that the effective propellant ionization rate, $\frac{\int \sigma_I f_e \mathrm{dv}}{\int f_e \mathrm{dv}} \approx const$ as well. Thus the expression under the integral in (2) is reduced by an order of magnitude in our range of voltages. The only possibility to compensate for that is to increase the area of integration (i.e., with substantial ionization) by the same factor. This tendency can be seen from Figs.10a, b, and also 13a, b, where contours of electron impact excitation are shown. The expansion of the layer can be seen from Figs. 9a, b as well.

The Dispersion Efficiency (reflecting the single ion exit angles) has an interesting and not fully understood behavior. For constant B, it increases slightly with voltage, apparently reflecting a slower-than-proportional increase of electron temperature with voltage. But at optimum B, the trend is clearly reversed. Further analysis of this and of its relationship to beam divergence is needed.

5. Conclusions and Recommendations

We have carried out a numerical exploration with a fully kinetic PIC code of the effects of raising the operating potential in a miniature TAL thruster. The results appear to validate the usefulness of this numerical tool for identifying detailed trends and effects, but it is also apparent that various improvements are still needed. Among them are elimination or reduction of the need for an artificially enlarged permittivity of vacuum, methods to speed up execution in general, transition to a ceramic-wall type of thruster, addition of higher than second ionization and addition of at least one ion excited level. Work is already underway on most of these points.

Among the important results of our work, we can mention:

- the calculation of the optimum magnetic field at each voltage,
- the existence of a maximum efficiency if the magnetic field is not optimized,
- the disappearance (or near disappearance) of this maximum when the magnetic field is optimized,
- the nearly linear increase of electron temperature with voltage,
- the spatial separation of the two channels for double ion formation, with one of them predominating in the low-potential central spike,
- the identification of most of the detailed mechanisms for efficiency variation, through a detailed analysis of its constitutive factors

We recommend implementation of the model improvements mentioned above, along with continued development of more advanced numerical techniques, and with appropriate experiments to be critically compared to these theories. A new such experiment which our results suggest would be spectroscopic examination of the spike region to verify the prediction of abundant double ions there.

References

[1] Oleson, S.R., Sankovic, J.M., "Advanced Hall Electric Propulsion for Future In-Space Transportation". NASA TM-2001-210676.

[2] Tverdokhlebov, S.O. and Garkusha, V.I., "High-Voltage Mode of the TAL Thruster Operation," Paper No. 97-023, 25th IEPC Conference, Cleveland, OH.

[3] Belikov, M.B., Gorskov, O.A., Rizakhanov, R.N., "Investigation of a Hall Thruster of 1.5 kW Class at Specific Impulses up to 3000s." Paper AIAA-2000-3253m 36th Joint Propulsion Conference, Huntsville, AL, July 2000.

[4] Pote, B., "Performance of a High Specific Impulse Hall Thruster," IEPC-01-35, 27th International Electric Propulsion Conference, Pasadena, CA, October 2001.

[5] Jacobson, D.T., Jankovsky, R.S., Rawlin, V.K. and Manzella, D.H., "High Voltage TAL Performance," Paper AIAA-2001-3777, 37th Joint Propulsion Conference, Salt Lake City, UT, July 2001.

[6] Manzella, D.H., Jacobson, D.T. and Jankowsky, R.S., “High Voltage SPT Performance”, Paper AIAA-2001-3774, 37th Joint Propulsion Conference, Salt Lake City, UT, July 2001.
[7] Grishin, S.D., Erofeev, V.S., Zharinov, A.V., Naumkin, V.P. and Safronov, I.N., “Characteristics of a Two-Stage Ion Accelerator with an Anode Layer.” Zhournal Prikladnoi Mekhaniki I Tekznicheskoi Fiziki, No. 2, pp. 28-36, March-April 1978.
[8] Tverdoklebov, S., “Study of Double-Stage Thrusters using Inert Gases”, Paper IEPC-93-232, 23rd International Electric Propulsion Conference, Seattle, WA, Sep. 1993.
[9] Semenkin S., Tverdoklebov, S. and Solodukhin, A., “Current Status of Multi-Mode TAL Development”. Paper AIAA-2001-3779, 37th Joint Propulsion Conference, Salt Lake City, UT, July 2001.
[10] Szabo, J.J., Martinez-Sanchez, M. and Batischev, O., “Numerical Modeling of the Near-Anode Region of a TAL Thruster’. Paper AIAA 2000-3653, 36th Joint Propulsion Conference, Huntsville, AL, July 2000.
[11] Szabo, J.J., Fully Kinetic Numerical Modeling of a Plasma Thruster, Ph.D. Thesis, MIT, Jan. 2001.
[12] Szabo, J.J., “Fully Kinetic Hall Thruster Modeling.” Paper IEPC-01-341, 27th International Electric Propulsion Conference, Pasadena, CA, Oct. 2001.
[13] E. Ahedo, P. Martinez-Cerezo, J.M. Gallardo and M. Martinez-Sanchez, “Characterization of the Plasma in a Hall Thruster”, Paper IEPC-01-17, 27th International Electric Propulsion Conference, Pasadena, CA, Oct. 2001.

Table 2. PIC computation results for the mini-TAL thruster at different voltages, magnetic fields and mass flow

			300	**300**	300	300	600	**600**	600	600	900	900	900	**900**	900	1200	1200	1200	**1200**	1200	600
Mass flow (mg/s)			0.1	**0.1**	0.1	0.1	0.1	**0.1**	0.1	0.1	0.1	0.1	0.1	**0.1**	0.1	0.1	0.1	0.1	**0.1**	0.1	0.167
B field (relative to nominal)			0.35	**0.5**	0.7	1	0.7	**1**	1.4	2	0.87	1	1.22	**1.41**	1.72	1	1.4	1.72	**2**	2.3	1
Currents (A)																					
	cathode		0.0732	**0.0693**	0.0677	0.0651	0.0744	**0.0766**	0.0823	0.0782	0.0803	0.0768	0.0790	**0.0826**	0.0802	0.0800	0.0789	0.0797	**0.0810**	0.0826	0.1348
	anode		0.0737	**0.0693**	0.0676	0.0649	0.0742	**0.0771**	0.0818	0.0782	0.0804	0.0770	0.0787	**0.0826**	0.0802	0.0804	0.0791	0.0789	**0.0802**	0.0831	0.1330
	beam		0.0599	**0.0647**	0.0663	0.0670	0.0707	**0.0773**	0.0846	0.0837	0.0765	0.0752	0.0789	**0.0824**	0.0835	0.0747	0.0779	0.0807	**0.0835**	0.0850	0.1500
	ionization		0.0793	**0.0747**	0.0764	0.0803	0.0765	**0.0829**	0.0896	0.0892	0.0817	0.0792	0.0826	**0.0871**	0.0853	0.0811	0.0821	0.0836	**0.0849**	0.0887	0.1551
Mass flows (mg/s)																					
	neutrals		0.0221	**0.0218**	0.0222	0.0221	0.0121	**0.0128**	0.0106	0.0118	0.0104	0.0101	0.0092	**0.0078**	0.0072	0.0097	0.0080	0.0074	**0.0059**	0.0049	0.0171
	ions	total	0.0737	**0.0792**	0.0805	0.0799	0.0860	**0.0924**	0.0983	0.0957	0.0925	0.0907	0.0939	**0.0971**	0.0971	0.0903	0.0925	0.0945	**0.0965**	0.0969	0.1704
		single	0.0659	**0.0703**	0.0706	0.0685	0.0755	**0.0794**	0.0813	0.0774	0.0809	0.0790	0.0804	**0.0819**	0.0805	0.0788	0.0789	0.0790	**0.0792**	0.0780	0.1365
		double	0.0079	**0.0089**	0.0098	0.0114	0.0104	**0.0130**	0.0170	0.0184	0.0116	0.0117	0.0135	**0.0152**	0.0167	0.0115	0.0136	0.0155	**0.0172**	0.0189	0.0340
Thrust (mN)																					
	ions	total	1.190	**1.274**	1.255	1.185	1.877	**2.013**	2.078	1.840	2.440	2.395	2.484	**2.586**	2.529	2.719	2.840	2.900	**2.949**	2.948	3.612
		single	1.017	**1.084**	1.058	0.978	1.577	**1.655**	1.642	1.418	2.040	1.994	2.029	**2.080**	1.996	2.268	2.311	2.310	**2.305**	2.252	2.773
		double	0.173	**0.190**	0.197	0.207	0.300	**0.358**	0.436	0.422	0.401	0.401	0.454	**0.506**	0.533	0.451	0.529	0.590	**0.643**	0.696	0.839
	neutrals		0.057	**0.052**	0.048	0.045	0.048	**0.038**	0.029	0.028	0.052	0.046	0.342	**0.027**	0.021	0.051	0.034	0.275	**0.019**	0.014	0.063
Isp (s)			1276	**1356**	1328	1252	1961	**2087**	2141	1903	2536	2483	2567	**2659**	2600	2822	2928	2982	**3023**	3023	2255
Average electron temp (eV)			13.5	**12.0**	11.4	12.1	17.8	**17.8**	19.6	21.8	24.9	24.7	25.2	**26.6**	28.5	32.5	33.1	34.6	**36.7**	37.9	19.2
Phi wall (V)			0.03	**0.00**	0.00	-0.01	-0.01	**-0.13**	-0.25	-0.31	0.00	-0.05	-0.15	**-0.23**	-0.41	0.00	-0.16	-0.32	**-0.55**	-0.88	-0.02
Densities in ioniz. region (cm-3)																					
	+ charges		2.66E+12	3.12E+12	3.32E+12	3.42E+12	2.62E+12	2.89E+12	2.66E+12	2.15E+12	2.40E+12	2.72E+12	2.47E+12	2.32E+12	1.88E+12	2.18E+12	2.03E+12	1.87E+12	1.59E+12	1.50E+12	3.64E+12
	neutrals		4.51E+13	3.92E+13	4.06E+13	3.73E+13	3.18E+13	1.57E+13	6.60E+12	3.91E+12	2.81E+13	2.04E+13	7.96E+12	4.43E+12	1.28E+12	2.43E+13	5.55E+12	1.54E+12	8.90E+11	9.46E+10	1.49E+13
Total mass (mg)																					
	ions		3.78E-08	3.99E-08	4.21E-08	4.55E-08	2.95E-08	3.04E-08	3.09E-08	3.29E-08	2.58E-08	2.48E-08	2.48E-08	2.41E-08	2.27E-08	8.36E-07	2.08E-08	2.02E-08	1.91E-08	1.86E-08	5.40E-08
	neutrals		1.02E-06	1.02E-06	1.04E-06	1.06E-06	8.85E-07	8.70E-07	8.27E-07	8.36E-07	8.46E-07	8.51E-07	8.29E-07	8.08E-07	7.91E-07	2.21E-08	8.05E-07	7.85E-07	7.70E-07	7.61E-07	1.28E-06
Efficiencies																					
	electrical		0.818	**0.933**	0.979	1.03	0.951	**1.01**	1.03	1.07	0.952	0.978	0.998	**0.998**	1.04	0.935	0.987	1.01	**1.03**	1.03	1.11
	single ions																				
		utilization	0.687	**0.695**	0.688	0.671	0.77	**0.755**	0.746	0.719	0.786	0.784	0.78	**0.781**	0.771	0.788	0.785	0.776	**0.774**	0.766	0.728
		acceler.	0.629	**0.629**	0.597	0.549	0.576	**0.583**	0.568	0.488	0.561	0.565	0.571	**0.584**	0.574	0.55	0.576	0.584	**0.592**	0.591	0.572
		dispersion	0.86	**0.859**	0.852	0.842	0.857	**0.846**	0.816	0.78	0.855	0.852	0.844	**0.835**	0.81	0.855	0.844	0.828	**0.81**	0.801	0.818
	double ions																				
		utilization	0.0822	**0.0885**	0.0958	0.112	0.106	**0.124**	0.156	0.171	0.113	0.116	0.131	**0.145**	0.16	0.115	0.135	0.152	**0.168**	0.186	0.181
		beta	1.42	**1.37**	1.34	1.27	1.38	**1.32**	1.27	1.25	1.37	1.36	1.33	**1.31**	1.29	1.36	1.33	1.31	**1.28**	1.27	1.22
	neutrals																				
		utilization	0.2308	**0.2165**	0.2162	0.217	0.124	**0.121**	0.098	0.11	0.104	0.1	0.089	**0.074**	0.069	0.097	0.08	0.072	**0.058**	0.048	0.091
		beta	0.167	**0.155**	0.145	0.144	0.191	**0.143**	0.135	0.131	0.199	0.181	0.147	**0.139**	0.115	0.181	0.147	0.128	**0.114**	0.101	0.182
	effective utilization		0.8332	**0.8282**	0.817	0.7968	0.8997	**0.8734**	0.8663	0.8455	0.9135	0.9068	0.898	**0.899**	0.8899	0.909	0.9035	0.8971	**0.8931**	0.8912	0.855
	Overall		0.3687	**0.4175**	0.4068	0.3794	0.4224	**0.4351**	0.4136	0.3444	0.4171	0.4269	0.4319	**0.4375**	0.4303	0.3997	0.4335	0.4382	**0.4411**	0.4345	0.4441

Appendix: Efficiency definitions

The overall efficiency of a Hall thruster is defined by:

$$\eta = \frac{T^2}{2mIV} \tag{A1}$$

where I is the cathode/anode current. It can be expressed as a function of the beam current:

$$I = \frac{I_{beam}}{\eta_e} \tag{A2}$$

where η_e is the electrical efficiency, and I_{beam} the ion beam current

$$I_{beam} = \frac{e}{m_i}\left(m^+ + 2m^{++}\right) \tag{A3}$$

Equation (A1) becomes

$$\eta = \eta_e \frac{T^2}{\frac{2mVe}{m_i}\left(m^+ + 2m^{++}\right)} \tag{A4}$$

The thrust T and the current I in (A4) are functions of the mass flows and average axial velocities of the different species: neutrals, single and double ions.

$$\eta = \eta_e \frac{\left(m^+\left\langle v_z^+\right\rangle + m^{++}\left\langle v_z^{++}\right\rangle + m^n\left\langle v_z^n\right\rangle\right)^2}{\frac{2mVe}{m_i}\left(m^+ + 2m^{++}\right)} \tag{A5}$$

This can also be written as

$$\eta = \eta_e \frac{m_i\left\langle v_z^+\right\rangle^2}{2Ve} \frac{\left(\frac{m^+}{m} + \frac{m^{++}}{m}\frac{\left\langle v_z^{++}\right\rangle}{\left\langle v_z^+\right\rangle} + \frac{m^n}{m}\frac{\left\langle v_z^n\right\rangle}{\left\langle v_z^+\right\rangle}\right)^2}{\left(\frac{m^+}{m} + 2\frac{m^{++}}{m}\right)} \tag{A6}$$

Introducing the acceleration and dispersion efficiency for the single ions,

$$\eta_a^+ = \frac{m_i\left\langle v^+\right\rangle^2}{2Ue} \tag{A7}$$

$$\eta_d^+ = \left(\frac{\left\langle v_z^+\right\rangle}{\left\langle v^+\right\rangle}\right)^2 \tag{A8}$$

equation (A6) becomes

$$\eta = \eta_e\eta_a^+\eta_d^+ \frac{\left(\frac{m^+}{m} + \frac{m^{++}}{m}\frac{\left\langle v_z^{++}\right\rangle}{\left\langle v_z^+\right\rangle} + \frac{m^n}{m}\frac{\left\langle v_z^n\right\rangle}{\left\langle v_z^+\right\rangle}\right)^2}{\left(\frac{m^+}{m} + 2\frac{m^{++}}{m}\right)} \tag{A9}$$

The utilization efficiencies for the single and double ions are defined by

$$\eta_u^+ = \frac{m^+}{m} \tag{A10}$$

$$\eta_u^{++} = \frac{m^{++}}{m} \tag{A11}$$

$$\eta_u^n = \frac{m^n}{m} = 1 - \frac{m^+ + m^{++}}{m} \tag{A12}$$

To characterize the acceleration and the dispersion of the neutrals and double ions, we introduce two parameters β^{++} and β^n,

$$\beta^{++} = \frac{\left\langle v_z^{++}\right\rangle}{\left\langle v_z^+\right\rangle} \tag{A13}$$

$$\beta^n = \frac{\left\langle v_z^n\right\rangle}{\left\langle v_z^+\right\rangle} \tag{A14}$$

Including these coefficients in η,

$$\eta = \eta_e\eta_a^+\eta_d^+ \frac{\left(\eta_u^+ + \eta_u^{++}\beta^{++} + \eta_u^n\beta^n\right)^2}{\left(\eta_u^+ + 2\eta_u^{++}\right)} \tag{A15}$$

For cases without double ions and neglecting the neutral thrust,

$$\eta = \eta_e\eta_a^+\eta_d^+\eta_u^+ \tag{A16}$$

For the case with double ions η can be expressed in a similar way if we define an efficient utilization η_u^{eff}:

$$\eta = \eta_e\eta_a^+\eta_d^+\eta_u^{eff} \tag{A17}$$

$$\eta_u^{eff} = \frac{\left(\eta_u^+ + \eta_u^{++}\beta^{++} + \eta_u^n\beta^n\right)^2}{\left(\eta_u^+ + 2\eta_u^{++}\right)} \tag{A18}$$